

This discussion paper is/has been under review for the journal Atmospheric Measurement Techniques (AMT). Please refer to the corresponding final paper in AMT if available.

# Estimation of waste water treatment plant methane emissions: methodology and results from a short campaign

C. E. Yver-Kwok<sup>1</sup>, D. Müller<sup>2</sup>, C. Caldw<sup>3</sup>, B. Lebegue<sup>1</sup>, J. G. Mønster<sup>4</sup>,  
C. W. Rella<sup>5</sup>, C. Scheutz<sup>4</sup>, M. Schmidt<sup>1</sup>, M. Ramonet<sup>1</sup>, T. Warneke<sup>2</sup>, G. Broquet<sup>1</sup>,  
and P. Ciais<sup>1</sup>

<sup>1</sup>Laboratoire des Sciences du Climat et l'Environnement (LSCE/IPSL), UMR8212, CNRS-CEA-UVSQ, Centre d'Etudes Orme des Merisiers, Gif sur Yvette, France

<sup>2</sup>Institute of Environmental Physics, University of Bremen, Otto-Hahn-Allee 1, 28359 Bremen, Germany

<sup>3</sup>Centre for Atmospheric Chemistry, University of Wollongong, Wollongong, NSW, 2522, Australia

<sup>4</sup>Department of Environmental Engineering, Technical University of Denmark, Bygningstorvet-Building 115, 2800 Lyngby, Denmark

<sup>5</sup>Picarro Inc., 3105 Patrick Henry Drive, Santa Clara, CA, USA

Title Page

Abstract

Introduction

Conclusions

References

Tables

Figures

◀

▶

◀

▶

Back

Close

Full Screen / Esc

Printer-friendly Version

Interactive Discussion



Received: 2 August 2013 – Accepted: 12 October 2013 – Published: 29 October 2013

Correspondence to: C. E. Yver-Kwok (camille.yver@lsce.ipsl.fr)

Published by Copernicus Publications on behalf of the European Geosciences Union.

**AMTD**

6, 9181–9224, 2013

---

**CH<sub>4</sub> local emissions  
measurements**

C. E. Yver-Kwok et al.

---

Title Page

Abstract

Introduction

Conclusions

References

Tables

Figures



Back

Close

Full Screen / Esc

Printer-friendly Version

Interactive Discussion



## Abstract

This paper describes different methods to estimate methane emissions at different scales. These methods are applied to a waste water treatment plant (WWTP) located in Valence, France. We show that Fourier Transform Infrared (FTIR) measurements as well as Cavity Ring Down Spectroscopy (CRDS) can be used to measure emissions from the process to the regional scale. To estimate the total emissions, we investigate a tracer release method (using  $C_2H_2$ ) and the Radon tracer method (using  $^{222}Rn$ ). For process-scale emissions, both tracer release and chamber techniques were used. We show that the tracer release method is suitable to quantify facility- and some process-scale emissions, while the Radon tracer method encompasses not only the treatment station but also a large area around. Thus the Radon tracer method is more representative of the regional emissions around the city. Uncertainties for each method are described. Applying the methods to  $CH_4$  emissions, we find that the main source of emissions of the plant was not identified with certainty during this short campaign, although the primary source of emissions is likely to be from solid sludge. Overall, the waste water treatment plant represents a small part (3 %) of the methane emissions of the city of Valence and its surroundings, which is in agreement with the national inventories.

## 1 Introduction

Human activities cause greenhouse gases (GHGs) emissions at a large scale, changing the atmospheric chemical composition by measurable and consequential amounts. Anthropogenic GHG emissions such as methane ( $CH_4$ ) now represent a significant fraction of total greenhouse gas emissions into the atmosphere. To better understand the anthropogenic sources of GHGs, with the goal of ultimately reducing these emissions, it is essential to accurately quantify the emissions at all spatial scales, from the process scale to the country scale. Two methods for estimating emissions are used: the

AMTD

6, 9181–9224, 2013

## $CH_4$ local emissions measurements

C. E. Yver-Kwok et al.

Title Page

Abstract

Introduction

Conclusions

References

Tables

Figures

◀

▶

◀

▶

Back

Close

Full Screen / Esc

Printer-friendly Version

Interactive Discussion



**CH<sub>4</sub> local emissions measurements**

C. E. Yver-Kwok et al.

Title Page

Abstract

Introduction

Conclusions

References

Tables

Figures

◀

▶

◀

▶

Back

Close

Full Screen / Esc

Printer-friendly Version

Interactive Discussion



top-down approach based on atmospheric measurements of GHGs at all scales and the bottom-up approach, which goes from the process scale to the global scale. Here, activity data, emission factors and flux modeling are used to calculate emissions. Primary sources of anthropogenic methane emissions are landfills, waste water treatment plants, rice paddies, ruminants and manure management, oil and gas production and transport activities. Combining the two approaches by using top down measurements at all scales to validate benchmark bottom-up calculations and emission factors can help not only improve inventories, but provide valuable information for how to prioritize emission reduction activities. In France, methane emissions from waste management (water treatment and landfills) accounted for about 19 % of the total methane emissions in 2011 (CITEPA, 2013). Landfills are the largest emitter with 17 %, but waste water treatment plants still represent a non-negligible part (2 %). However, these values are estimated with 100 % uncertainty due to the difficulty to accurately estimate the terms used in the equation to compute emissions (biological demand in oxygen (BOD), quantity of CH<sub>4</sub> emitted by kg of BOD, fraction of treated incoming wastewater, anoxic/oxic conditions) (CITEPA, 2013). Several studies have been conducted in different countries to provide more accurate estimates of the emissions for WWTPs. Cakir and Stenstrom (2005); El-Fadel and Massoud (2001) present estimations based on process modeling, but some studies such as Czepiel et al. (1993); Wang et al. (2011); Daelman et al. (2012) calculate emissions using CH<sub>4</sub> measurements with mass budget. In these papers, emissions vary from 0.011 to 0.309 kg yr<sup>-1</sup> per inhabitant depending on the WWTP design (e.g., aerobic or anaerobic processes, presence of a sludge digester). For municipal waste water treatment plants using activated sludge (aerobic) treatment, emissions still vary from 0.039 to 0.309 kg yr<sup>-1</sup> per inhabitant. In this study, we present different methods – chamber measurements, dual tracer method with acetylene and Radon – to calculate GHG emissions at the process to the plant scale and with the Radon dual tracer method to extend the calculations to the surrounding area. We focus on CH<sub>4</sub> from a municipal waste water plant that employs activated sludge treatment, but the methodology could be applied to other point sources such as landfills, and other



**CH<sub>4</sub> local emissions measurements**

C. E. Yver-Kwok et al.

Title Page

Abstract

Introduction

Conclusions

References

Tables

Figures

◀

▶

◀

▶

Back

Close

Full Screen / Esc

Printer-friendly Version

Interactive Discussion



We anticipated the potential for methane release during all steps of the process. In the aeration basins, periods of aeration with aerobic reaction alternate with rests where anaerobic reactions can occur. Methane formed during these resting phases is then transported to the surface when aeration restarts and provokes a mixing of water.

In the degassing pond, water is mixed and dissolved methane can be released. In the clarification tank, as there is a slow mixing, some degassing could still be expected, with bacteria from the active sludge still producing methane. Finally, the sludge may still contain methane that could be emitted during centrifugation, storage and incineration. In addition, methane dissolved in the incoming water from the city will be released at the plant, starting from the first exposure to the atmosphere, and certainly during the aeration process.

## 2.2 Instruments

During this one week campaign, two FTIR analyzers measuring CO<sub>2</sub>, CH<sub>4</sub>, N<sub>2</sub>O, CO and δ<sup>13</sup>C in CO<sub>2</sub>, one CRDS instrument (custom prototype, Picarro Inc. Santa Clara) measuring CH<sub>4</sub>, CO<sub>2</sub> and H<sub>2</sub>O or C<sub>2</sub>H<sub>2</sub>, CH<sub>4</sub> and H<sub>2</sub>O, a radon analyzer and a weather station were installed to measure GHG concentrations and estimate emissions (see Fig. 1 and Table 1). The radon analyzer and the weather station measured at the same location throughout the campaign. One of the FTIR analyzers was used to measure samples from the ponds and the second mostly sampled air at the same location as the Radon analyzer but performed some measurements above the ponds as well. The CRDS instrument was installed in a car along with a real time GPS device and was thus mobile.

### 2.2.1 FTIR analyzers

An FTIR analyzer records a spectrum over a broad IR range (1800–5000 cm<sup>-1</sup>), thereby offering the possibility to measure a large number of species simultaneously. Spectra are stored and can be analyzed at a later date with a different method to

**CH<sub>4</sub> local emissions measurements**

C. E. Yver-Kwok et al.

Title Page

Abstract

Introduction

Conclusions

References

Tables

Figures

◀

▶

◀

▶

Back

Close

Full Screen / Esc

Printer-friendly Version

Interactive Discussion



get data with a higher accuracy or study new species. In the FTIR, the infrared signal passes first through a Michelson interferometer, then this modulated beam traverses the sample cell. The resulting time-modulated signal is then converted into an infrared spectrum through Fourier transform. The FTIR analyzer operated by the LSCE is a commercially available Ecotech instrument. The instrument operated by the Bremen University was built at the University of Wollongong, Australia. Both instruments are functionally identical. A detailed description is found in Griffith et al. (2012); Hammer et al. (2012). Here, we briefly describe the instruments as used during the campaign. Both were installed in small shelters without air conditioning. The first one, operated by LSCE, was installed to sample ambient air above the whole station for the majority of the time. During the last day, air was sampled above different basins with this instrument. The second FTIR was operated by the Bremen University, and was used to analyze samples from a floating chamber operated in the clarification and the aeration basins. Each of the two instruments consists of a commercially available FTIR interferometer (IRcube, Bruker Optics, Germany) with a  $1\text{ cm}^{-1}$  resolution coupled with a 3.5 L multi-pass cell with a 24 m optical path length (PA-24, InfraredAnalysis, Anaheim, USA). The cell and the interferometer are put together on an optical bench inside a temperature controlled chamber. An in-situ PT100 platinum resistance thermometer (RTD) and a pressure sensor (HPM-760s, Teledyne Hastings, USA) are installed on the multi-pass cell. High purity nitrogen (grade 4.5) is used to purge the interferometer housing as well as the transfer-optics between the cell and the interferometer. A drying system composed of a 24 inch counter-flow Nafion dryer (Permapure, Toms River, NJ, USA) followed by a chemical dryer ( $\text{Mg}(\text{ClO}_4)_2$ ) was located upstream from the cell.

For the LSCE instrument, the pressure of the cell is controlled using a mass flow sensor mounted at the outlet of the cell, and the flow is controlled by another mass flow controller installed upstream from the drying system. Four reference gases and a control gas were used regularly during the five days of the campaign for calibration (once a day, 45 min for each calibration gas) and quality control (every 3–4 h). During these five days, the temperature inside the shelter sometimes exceeded  $30^\circ\text{C}$ . In or-



**CH<sub>4</sub> local emissions measurements**

C. E. Yver-Kwok et al.

Title Page

Abstract

Introduction

Conclusions

References

Tables

Figures

◀

▶

◀

▶

Back

Close

Full Screen / Esc

Printer-friendly Version

Interactive Discussion



was added. Three separate lasers are used in this spectrometer. Light from each laser, tuned to specific near-infrared absorption features of the key analyte molecules, is directed sequentially into an optical resonator (called the optical cavity). The optical cavity consists of a closed chamber with three highly reflective mirrors, and it serves as a compact flow cell with a volume of less than 10 standard cm<sup>3</sup> into which the sample gas is introduced. The flow cell has an effective optical path length of 15–20 km; this long path length allows for measurements with high precision (with ppb or even parts-per-trillion uncertainty, depending on the analyte gas), using compact and highly reliable near-infrared laser sources. The gas temperature and pressure are tightly controlled in these instruments (Crosson, 2008). This stability allows the instrument (when properly calibrated to traceable reference standards) to deliver accurate measurements that need very infrequent calibration relative to other CO<sub>2</sub> and CH<sub>4</sub> instrumentation.

The instrument employs precise monitoring and control of the optical wavelength, which delivers sub-picometer wavelength targeting on a microsecond timescale. Ring-down events are collected at a rate of about 200 ringdowns s<sup>-1</sup>. Individual spectrograms consist of about 50–100 individual ringdowns (or 0.25–0.5 s), distributed across 10–20 spectral points around the peak. The overall measurement interval is about 1 s. The resulting spectrograms are analyzed using nonlinear spectral pattern recognition routines, and the outputs of these routines are converted into gas concentrations using linear conversion factors derived from calibration using gravimetric standards or other artifact standards. There are two modes of operation for this analyzer: a C<sub>2</sub>H<sub>2</sub>/CH<sub>4</sub>/H<sub>2</sub>O mode, and a CO<sub>2</sub>/CH<sub>4</sub>/H<sub>2</sub>O mode. The spectroscopy of CO<sub>2</sub>, CH<sub>4</sub> and H<sub>2</sub>O is identical to the algorithms that are used in several standard models from the same manufacturer (e.g., models G1301, G2301, G2401); the performance of these instruments for atmospheric measurements of CO<sub>2</sub>, CH<sub>4</sub>, and H<sub>2</sub>O has been described in detail elsewhere (Crosson, 2008; Chen et al., 2010; Winderlich et al., 2010; Rella et al., 2013; Fang et al., 2013). The basic performance reported in these papers should be highly representative of the performance of this analyzer. A series of laboratory tests were performed to establish the basic performance of the analyzer, consisting of continuous

**CH<sub>4</sub> local emissions measurements**

C. E. Yver-Kwok et al.

Title Page

Abstract

Introduction

Conclusions

References

Tables

Figures

◀

▶

◀

▶

Back

Close

Full Screen / Esc

Printer-friendly Version

Interactive Discussion



measurements on prepared gas mixtures. The uncertainty calculated from these tests is summarized in Table 1. The CH<sub>4</sub> measurements were calibrated using 4 gravimetrically prepared mixtures of methane with concentration ranging from 1.7 to 2.3 ppm, along with ultrapure nitrogen. The C<sub>2</sub>H<sub>2</sub> measurement was not calibrated directly with a standard. Instead, the spectroscopy calibration constant that was measured on another C<sub>2</sub>H<sub>2</sub> instrument that uses the same spectral line (Model G1203, SN: DFADS002, Picarro, Inc, Santa Clara) was applied to our measurements.

**2.2.3 Radon-222 analyzer**

Radon-222 (<sup>222</sup>Rn) is a natural radioactive gas in the uranium-238 decay series. <sup>222</sup>Rn is emitted by soils and is therefore more abundant above continental surfaces than over the oceans. The exhalation rate of <sup>222</sup>Rn changes with soil type and meteorological conditions such as atmospheric pressure, soil water content or precipitation (Schery et al., 1984). As a noble gas, <sup>222</sup>Rn is chemically inert and its mobility depends only on physical processes (diffusion, adsorption, advection). The variations of its concentration in the atmosphere depend thus mostly on the boundary layer height variations. Moreover, its half-life of 3.82 days makes <sup>222</sup>Rn a good tracer for regional atmospheric circulation studies. During the campaign, we used a radon analyzer lent and developed by the University of Heidelberg and described in detail in Levin et al. (2002). Briefly, the activity of the short-lived <sup>222</sup>Rn decay products, attached to aerosols, is accumulated on a quartz aerosol filter and assayed on line by  $\alpha$ -spectroscopy. This analyzer can measure <sup>222</sup>Rn activities every thirty minutes down to 0.5 Bq m<sup>-3</sup> with an uncertainty below  $\pm 20\%$ . The radon analyzer was installed on top of a building located between the measured ponds. The sampling height was approximately 7 m and next to the FTIR sampling outlet operated by LSCE.

Sampling began on 17 September at 17:00 GMT and finished on 21 September at 06:00 GMT. Due to instrument malfunction, no data were recorded between the 19 September from 08:30 GMT to the 20 September at 00:30 GMT and from the 20 September at 06:30 GMT to the 20 September at 17:30 GMT.

## 2.2.4 Weather station

A weather station (WXT520, Vaisala) was installed next to the FTIR and radon analyzer inlets. Wind speed, wind direction, temperature, relative humidity and atmospheric pressure were measured every second and averaged every minute.

## 3 Emission estimation methods

### 3.1 Chamber measurements on the basins

Depending on the basin areas under investigation, two different modes of chamber measurements were employed: (a) accumulation closed-chamber measurements (Frankignoulle, 1988) and (b) flow-through open-chamber measurements. The former mode was employed on the clarification pond (18 September) and on the aeration pond (19 September) outside of the aerated area of the basin, which had rather calm surfaces, and the latter on the aerated part of the aeration pond, where air is injected in the basin, resulting in a large air flux and turbulent surface (see Figs. 2 and 3).

#### 3.1.1 Accumulation (closed-chamber) measurements

The chamber is closed against ambient air and the mass flux  $F$  is calculated from the linear increase of the measured gas mole fraction in the chamber with time (see Fig. 3a):

$$F = \frac{\Delta C}{\Delta t} \frac{pVM A_{\text{pond}}}{RTA} \quad (1)$$

where  $\frac{\Delta C}{\Delta t}$  is the fitted linear increase of the gas mole fraction in the chamber with time ( $\text{mol mol}^{-1} \text{s}^{-1}$ ),  $p$  is the pressure in the floating chamber (atm),  $T$  the temperature (K),  $R$  the universal gas constant ( $0.0821 \text{ L atm K}^{-1} \text{ mol}^{-1}$ ),  $V$  represents the volume of the

Title Page

Abstract

Introduction

Conclusions

References

Tables

Figures

◀

▶

◀

▶

Back

Close

Full Screen / Esc

Printer-friendly Version

Interactive Discussion



chamber ( $L$ ),  $A$  the water surface area enclosed by the chamber ( $m^2$ ),  $A_{\text{pond}}$  the area of the pond ( $m^2$ ) and  $M$  the molar mass of methane ( $g\ mol^{-1}$ ).

### 3.1.2 Flow-through (open-chamber) measurements

The chamber was modified for flow-through measurements with small holes present in the top of the chamber to allow excess injected air to escape. During aeration times, the air in the chamber was replaced within a few minutes. Hence, the gas concentration in the chamber represented the concentration in the aeration air emitted from the pond, once several mixing times in the chamber volume had occurred. Therefore, the mass flux of the emitted gas was able to be calculated by the amount of injected air monitored by in-situ instruments operated by the WWTP, the gas concentration within the injected air and its integration over time (see Fig. 3b):

$$F = \sum C \frac{M}{V_m} \frac{dV_{\text{Aeration}}}{dt} \quad (2)$$

where  $C$  is the gas mole fraction ( $mol\ mol^{-1}$ ),  $\frac{dV_{\text{aeration}}}{dt}$  is the volume of air injected inside the chamber per time ( $m^3\ h^{-1}$ ),  $M$  is the molar mass of  $CH_4$  ( $g\ mol^{-1}$ ) and  $V_m$  is the molar volume of ideal gases ( $m^3\ mol^{-1}$ ).

### 3.2 Radon tracer method

The Radon tracer method is described in detail in several papers (Levin et al., 1999; Schmidt et al., 2001; Biraud et al., 2000; Messenger et al., 2008; Hammer and Levin, 2009; Yver et al., 2009). Briefly, gas fluxes can be estimated using a simple one-dimensional approach. Assuming that the gases (here  $CH_4$  and  $^{222}Rn$ ) are released from the atmosphere at a constant rate  $F$  in a well-mixed layer of height  $H$ , we can write the temporal variation of their concentration  $C$  (with an additional radioactive de-

## CH<sub>4</sub> local emissions measurements

C. E. Yver-Kwok et al.

Title Page

Abstract

Introduction

Conclusions

References

Tables

Figures

◀

▶

◀

▶

Back

Close

Full Screen / Esc

Printer-friendly Version

Interactive Discussion



day term for  $^{222}\text{Rn}$ ):

$$\frac{\Delta C}{\Delta t} = \frac{F}{H} \text{ for } \text{CH}_4 \quad (3)$$

$$\frac{\Delta C}{\Delta t} = \frac{F}{H} - \lambda C \text{ for } ^{222}\text{Rn} \quad (4)$$

5 with  $\lambda$  (in  $\text{s}^{-1}$ ) the radioactive decay coefficient for  $^{222}\text{Rn}$ . If we combine Eqs. (3) and (4), we eliminate the boundary layer height:

$$F_{\text{CH}_4} = F_{^{222}\text{Rn}} \frac{\Delta C_{\text{CH}_4}}{\Delta C_{^{222}\text{Rn}}} \left( 1 - \lambda_{^{222}\text{Rn}} \frac{C_{^{222}\text{Rn}} \Delta t}{\Delta C_{^{222}\text{Rn}}} \right) \quad (5)$$

10  $F_{^{222}\text{Rn}}$  is the mean  $^{222}\text{Rn}$  emission rate of the region of influence,  $\frac{\Delta C_{\text{CH}_4}}{\Delta C_{^{222}\text{Rn}}}$  is the slope of the linear regression of half-hourly observations between  $\text{CH}_4$  and  $^{222}\text{Rn}$  and  $(1 - \lambda_{^{222}\text{Rn}} \frac{C_{^{222}\text{Rn}} \Delta t}{\Delta C_{^{222}\text{Rn}}})$  is the factor used to correct for  $^{222}\text{Rn}$  radioactive decay. Schmidt et al. (2001) showed that during a typical night-time inversion situation lasting 8–12 h, the change in radon activity as a result of radioactive decay, offset by fresh emission from soil, was only 3–4 %. On the basis of this work, we used a correction factor of 0.965. In this approach, the gas fluxes are considered collocated spatially and temporally, with  
15 no mixing of air from the free troposphere. Here, as  $\text{CH}_4$  is emitted from the installations and not from the soil, we make the assumption that we sample air high enough for the emissions to be seen as collocated. It is however a strong assumption, as the  $^{222}\text{Rn}$  sources are diffuse and the closest  $\text{CH}_4$  sources are so close (i.e. the emissions from the station). The boundary layer height and the gas fluxes are assumed to remain  
20 constant during each event.  $F_{\text{Rn}}$  is evaluated using the  $^{222}\text{Rn}$  European map available at <http://radon.unibas.ch/> and described in Szegvary et al. (2009). The average flux for the pixels surrounding the station reaches  $74 \text{ Bq m}^{-2} \text{ h}^{-1}$ . Schmidt et al. (2001); Yver et al. (2009) have estimated the error on the  $^{222}\text{Rn}$  flux to be less than 25 % for

## CH<sub>4</sub> local emissions measurements

C. E. Yver-Kwok et al.

Title Page

Abstract

Introduction

Conclusions

References

Tables

Figures

◀

▶

◀

▶

Back

Close

Full Screen / Esc

Printer-friendly Version

Interactive Discussion



## CH<sub>4</sub> local emissions measurements

C. E. Yver-Kwok et al.

Title Page

Abstract

Introduction

Conclusions

References

Tables

Figures

◀

▶

◀

▶

Back

Close

Full Screen / Esc

Printer-friendly Version

Interactive Discussion



France and the Ile-de-France region using soil map and measurements in France and in Germany. We can reasonably assume the same uncertainty here. The total error on the method is composed of the error of the flux, the error of the decay term and the errors in measurements of CH<sub>4</sub> and <sup>222</sup>Rn. Schmidt et al. (2001) estimated the error on the decay term to be 7 %. The errors on the measurements are usually less than 1 % for CH<sub>4</sub> and less than 20 % for <sup>222</sup>Rn which give us a total error of about 25 %. During the campaign, measurements of CH<sub>4</sub> from the LSCE FTIR analyzer and <sup>222</sup>Rn sampled at the same location were analyzed. Events when CH<sub>4</sub> and <sup>222</sup>Rn seemed correlated were selected and the Pearson correlation coefficient calculated. If it was higher than 0.6, we calculated the emissions.

### 3.3 Tracer release method

The tracer release method consists in releasing a tracer gas (here C<sub>2</sub>H<sub>2</sub>) at a known rate from a location which is collocated with the unknown emission of a trace gas to be determined, here CH<sub>4</sub>. This method has often been used in previous studies to determine CH<sub>4</sub> from landfills (Czepiel et al., 1996; Galle et al., 2001; Spokas et al., 2006; Fredenslund et al., 2010). Concentrations of the tracer as well as the gas of interest are measured using a mobile instrument downwind in the co-propagating plumes. The ratio of the area of the two plumes signals is proportional to the emission rate. Thus, knowing the emission rate of the released gas and the concentrations of both gases, we can calculate the emission rate of the gases of interest:

$$F_{\text{CH}_4} = F_{\text{C}_2\text{H}_2} \frac{A_{\text{CH}_4}}{A_{\text{C}_2\text{H}_2}} \frac{M_{\text{CH}_4}}{M_{\text{C}_2\text{H}_2}} \quad (6)$$

with  $F_{\text{CH}_4}$  the emissions of CH<sub>4</sub> (kg h<sup>-1</sup>),  $F_{\text{C}_2\text{H}_2}$ , the known emissions of C<sub>2</sub>H<sub>2</sub> (kg h<sup>-1</sup>),  $\frac{A_{\text{CH}_4}}{A_{\text{C}_2\text{H}_2}}$  the ratio of the areas under the signals of CH<sub>4</sub> and C<sub>2</sub>H<sub>2</sub> and  $\frac{M_{\text{CH}_4}}{M_{\text{C}_2\text{H}_2}}$  the ratio of the molar masses of CH<sub>4</sub> and C<sub>2</sub>H<sub>2</sub>. As for the Radon tracer method, the emission

sources have to be collocated in time and space. For stationary experiments, Eq. (6) is modified such that the slope of the  $\text{CH}_4$  versus  $\text{C}_2\text{H}_2$  linear correlation is used to calculate the unknown flux instead of the area under the signals.

In this study, a 50 L cylinder of  $\text{C}_2\text{H}_2$  was situated next to the degassing pond, and the experiment repeated twice under two different wind conditions. On 18 September, the wind was coming from the south pushing the plumes in the direction of a nearby bridge across the Rhône. About 10 transects of the plumes were performed. Later that day, a stationary experiment was performed to measure the emissions from the degassing pond with the car parked about 65 m away from it. On 19 September, the wind was stronger and coming from the north. The instruments were driven along the roads south of the station to cross the plume. Finally, a last experiment with the  $\text{C}_2\text{H}_2$  cylinder close to the clarification pond, and thus located more centrally to the station was conducted.

In this method, uncertainties are coming from the concentrations, the tracer flux and the correlation between the plumes.  $\text{CH}_4$  and  $\text{C}_2\text{H}_2$  errors are small, less than 2 % and 10 % respectively for one minute average. Once the gas cylinder is installed and regulated, the flow of tracer gas is steady and well-known and this error is negligible. The main uncertainties come from the non-collocation of the plumes and from the analysis of the plumes, especially the background determination for  $\text{CH}_4$  and the calculation of the areas. To estimate this latter error, we calculated the signal areas with two methods. In the first one, the background is defined as the 5th percentile of the data measured during the release. In the second one, the background for  $\text{CH}_4$  is graphically defined. Comparing the two results, discrepancies between the emissions range from 10 to 40 %. To estimate the non collocation error, we have run one experiment with the  $\text{C}_2\text{H}_2$  cylinder at a different location; however, due to the small amplitudes of the signal as well as the high noise, these data could not be used quantitatively. To reduce the error as much as possible, we drove away far enough as was convenient with the existing roads (500 to 1 km away) to consider the two signals punctual and collocated. We also discuss qualitatively this assumption in the following section. Finally, we chose signals

## $\text{CH}_4$ local emissions measurements

C. E. Yver-Kwok et al.

Title Page

Abstract

Introduction

Conclusions

References

Tables

Figures

◀

▶

◀

▶

Back

Close

Full Screen / Esc

Printer-friendly Version

Interactive Discussion



with a correlation coefficient between the CH<sub>4</sub> and C<sub>2</sub>H<sub>2</sub> concentrations composing the peak higher than 0.6, to ensure a balance between high correlation and number of selected events.

## 4 Results

### 4.1 Ambient air measurements

The CH<sub>4</sub> concentrations from the LSCE FTIR analyzer, the radon activity, the wind speed, the wind direction and the temperature measured during the whole campaign (except the sampling above the basins) is plotted in Fig. 4. CH<sub>4</sub> concentrations vary between 1900 and 2300 ppb. The gaps in the data correspond to calibration periods and sampling above the basins. The highest concentrations are observed on the first and last days matching stable air mass (almost no wind speed and fast changes in wind directions). On the 19 and 20 September, the wind direction is varying from north, north-east to south, south-east. Due to several gaps in the radon measurements, it is difficult to determine the degree to which the Radon correlates with CH<sub>4</sub>. However, the signals seem correlated during the first hours and the last hours of the 18 September. Wind speed varies between 0 and 10 ms<sup>-1</sup> with a diurnal cycle. Temperature follows a similar expected pattern varying between 10 and 24 °C.

During the last night, the CRDS and the FTIR analyzers were sampling next to each other. The comparison of the two is shown in Fig. 5. Contrary to the FTIR analyzer which was calibrated regularly during the entire campaign, the CRDS analyzer was calibrated only once before the in-situ measurements. However, a good agreement is observed between the two instruments with a mean difference of  $2.4 \pm 3.9$  ppb (standard deviation). The WMO recommendation for laboratory intercomparison is < 2 ppb in background air (WMO, 2011). We can then reasonably expect that if we calibrate the CRDS instrument more often, we would reach the recommended goal even for polluted air masses. As said before, additional FTIR measurements were performed.

## CH<sub>4</sub> local emissions measurements

C. E. Yver-Kwok et al.

Title Page

Abstract

Introduction

Conclusions

References

Tables

Figures

◀

▶

◀

▶

Back

Close

Full Screen / Esc

Printer-friendly Version

Interactive Discussion



Both FTIR analyzers measured CH<sub>4</sub> from the basins but at different times and using different methods. In Fig. 6, measurements above the clarification, aeration and degassing basins with the LSCE FTIR analyzer sampling outlet 50 cm above the basins are shown. For the aeration and the clarification ponds, the concentrations at the time of measurement are close to the concentrations measured for the whole station. However, above the degassing pond, elevated concentrations of CH<sub>4</sub> are measured, up to 4300 ppb.

## 4.2 Direct flux measurements with chambers

### 4.2.1 Clarification pond

Chamber placements aimed to capture spatial flux variations and covered three approximate positions as indicated in Fig. 2a. The clarification pond possessed a rotating arm, or mixer, that was used to gently stir the pond and encourage the drainage of benthic sludge towards and out of a central hole at the bottom of the pond. Whilst the mixer was on, the floating chamber was tethered to the rotating arm and moved very slowly with the arm. Consequently, whilst sampling, the chambers moved about one half to one full rotation around the pond. The movement-induced turbulence was assumed to have a negligible effect on the flux as the arm rotated at a slow rate, covering one rotation of 360° in approximately 30 min. During the floating chamber deployment (accumulation mode), the CH<sub>4</sub> concentration increased in the chamber over time. A total of eight successful chamber runs were made on the clarification pond.

Where possible (see discussion below), the increase was approximated by linear least-square fitting and the fluxes calculated. As for the errors, five main sources of uncertainty were considered. First, the error associated with the linear fit was taken into account and calculated as the coefficient of variation (CV). Secondly, the uncertainty associated with the volume of the chamber was considered. This uncertainty arises both from the initial measurement of the total volume of the chamber and from the uncertainty associated with the water level in the chamber. The latter would, thirdly, also

## CH<sub>4</sub> local emissions measurements

C. E. Yver-Kwok et al.

Title Page

Abstract

Introduction

Conclusions

References

Tables

Figures

◀

▶

◀

▶

Back

Close

Full Screen / Esc

Printer-friendly Version

Interactive Discussion



**CH<sub>4</sub> local emissions measurements**

C. E. Yver-Kwok et al.

Title Page

Abstract

Introduction

Conclusions

References

Tables

Figures

◀

▶

◀

▶

Back

Close

Full Screen / Esc

Printer-friendly Version

Interactive Discussion



affect the water surface area enclosed by the chamber. Here, it was assumed that the water level varied by 1 cm. The uncertainties associated with the pressure and temperature sensors were also considered in terms of the confidence interval provided by the manufacturer. The overall uncertainty was calculated using Gaussian error propagation. The uncertainty in volume and area contributed to the squared total error by 52 and 48 %, respectively, for all four diffusive flux measurements. The uncertainties associated with CV, pressure and temperature were negligible. The uncertainties of volume and surface area eventually depend on the uncertainty of the water level. Consequently, a more accurate measurement of the water level in the chamber and a minimization of its variation should be aimed at if lowering of the total uncertainty is desired.

Only 4 out of the 8 successful floating chamber measurements on the clarification pond exhibited a non-ambiguous linear increase (chamber runs 2 (from minute 7 on, see Fig. 7), 3, 4, 7). The emissions calculated from these measurements averaged  $0.006 \pm 0.0004 \text{ kg d}^{-1}$  (for the individual values see Table 2). The standard deviation, calculated to assess the spread of the individual measurements, was  $0.004 \text{ kg d}^{-1}$ . It is reasonable that upscaling to the whole pond introduces uncertainty when not all locations on the pond were covered by our measurements. Based on our four measurements, we consider the obtained average of  $0.006 \text{ kg d}^{-1}$  to give the order of magnitude of the diffusive exchange flux, which represents the lower limit of the total emissions from the clarification pond.

For the other four measurements, the increase cannot be linearly approximated and it is suggested that erratic methane emissions caused this non-linearity, e.g., ebullition. Since such events might occur more frequently close to the rotating arm and the number of measurements is too small for estimating the frequency of such events, it is difficult to estimate the methane flux from the pond generated by erratic events. However, we can state that the highest average flux for these measurements over a 10 min period is  $0.257 \pm 0.016 \text{ kg d}^{-1}$  (chamber run 5).

Overall it can be stated that the fluxes of methane were higher when the mixer was on and the arm rotated. The rotating arm extended down through the water column



## CH<sub>4</sub> local emissions measurements

C. E. Yver-Kwok et al.

Title Page

Abstract

Introduction

Conclusions

References

Tables

Figures

◀

▶

◀

▶

Back

Close

Full Screen / Esc

Printer-friendly Version

Interactive Discussion



(0.038 kg d<sup>-1</sup>) is a conservative estimate including the diffusive flux only, and would represent the lower limit of the total flux (diffusive + erratic) from this area. However, the fluxes are very different in the area where the aeration takes place. There, the floating chamber was operated in flow-through mode over night. Figure 8 shows the CH<sub>4</sub> mixing ratios in the chamber (upper panel) and the amount of injected air (lower panel). It can be seen that whenever the aeration starts, the methane concentration rises up to a maximum, and decreases already before the aeration stops. We think that during the phases when no air and thus no oxygen is injected, there is a buildup of methane in the pond. Once the aeration starts, the methane is emitted from the pond with the aeration air.

The night measurements cover approximately 13 h and are therefore believed to offer a reasonably good temporal coverage for upscaling. Accordingly,  $0.658 \pm 0.004$  kg d<sup>-1</sup> were emitted. This number is subject to a number of uncertainties and can only be seen as a rough estimate. The error was calculated from the uncertainty of the FTIR measurement only, the uncertainty associated with the volume of injected air was not considered, which is why the actual uncertainty is likely higher.

It can further be seen from Fig. 8, that the methane concentration maxima are lower during the late night than in the evening. In fact, an overall decrease of the maxima can be observed, along with shorter periods of non-aeration. Figure 9 indicates a linear correlation between the length of the non-aeration period and the methane maximum that is observed during the subsequent chamber measurement (correlation coefficient  $R = 0.86$ ). This supports our hypothesis that methane production occurs during non-aeration times, which is, in turn, responsible for the high methane emitted in the subsequent aeration phase.

### 4.3 Total emissions: tracer release and Radon tracer

Figure 10 presents measurements from CH<sub>4</sub> and C<sub>2</sub>H<sub>2</sub> during the four tracer release episodes. During the first episode, the wind was coming from the south. Using the

**CH<sub>4</sub> local emissions measurements**

C. E. Yver-Kwok et al.

Title Page

Abstract

Introduction

Conclusions

References

Tables

Figures

◀

▶

◀

▶

Back

Close

Full Screen / Esc

Printer-friendly Version

Interactive Discussion



close-by bridge above the Rhône, we transected the plumes about 10 times. During the stationary measurements of the second episode, the winds were south south-west. On the third episode, with northerly winds, we crossed the plumes 12 times driving south of the station. Finally, after moving the C<sub>2</sub>H<sub>2</sub> cylinder to a more central position, 3 measurements of the plume were done. However, due to the small amplitudes of the signal as well as the higher noise, these data are only used qualitatively. As shown in Fig. 11 on the right part, when the acetylene cylinder is located near the degassing pond (location A in Fig. 11), the two signals are shifted in time, depending on the direction we were driving. This shows that this location is not optimal to sample the methane emissions from the station when still close to it (about 800 m). Judging by the horizontal displacement of the plumes with respect to each other, and the direction of the wind, the methane source appears to be west of the degassing pond. Once the cylinder was moved to the clarification pond (location B), we can see a better correlation of the signals with no horizontal displacement, which indicates that the cylinder is located to the axis of the methane plume propagating in the direction of the wind.

It was not possible to measure the small degassing pond that feeds the clarification tanks using the floating chamber method, due to the obstructed access to this tank. However, the mobile CRDS CH<sub>4</sub>/C<sub>2</sub>H<sub>2</sub> instrument was used to quantify the emissions from this source. On 18 September, with winds originating from the SSW, driving both immediately upwind and downwind of this tank (within 10 m) and the nearby clarification tank, a clear and distinct plume from this tank was identified. No significant emissions were observed from any of the clarification tanks consistent with the floating chamber measurements. The C<sub>2</sub>H<sub>2</sub> gas cylinder was situated on the eastern edge of the degassing pond, about 7 m east of the center of the 5 m radius pond. The measurement vehicle was parked 65 m downwind of the degassing pond. This distance is about 9 times greater than the separation of the C<sub>2</sub>H<sub>2</sub> and CH<sub>4</sub> sources. We expect plumes should be reasonably mixed at this distance, especially given the strong afternoon turbulent mixing of the atmosphere when these measurements were made (see Fig. 4). Under these well mixed conditions, the static plume correlation method

## CH<sub>4</sub> local emissions measurements

C. E. Yver-Kwok et al.

Title Page

Abstract

Introduction

Conclusions

References

Tables

Figures

◀

▶

◀

▶

Back

Close

Full Screen / Esc

Printer-friendly Version

Interactive Discussion



can be employed to measure the relative emissions of CH<sub>4</sub> and C<sub>2</sub>H<sub>2</sub>. About half an hour of CH<sub>4</sub> and C<sub>2</sub>H<sub>2</sub> measurements were made at this location, with the wind wafting the plumes back and forth across the measurement location. The winds came reliably from the SSW during this time, meaning that the measurements were not polluted by methane from the aeration tanks or incineration building. The time series of C<sub>2</sub>H<sub>2</sub> and CH<sub>4</sub> are shown in Fig. 10. The signals are clearly correlated. We plot methane as function of C<sub>2</sub>H<sub>2</sub>, and fit the resulting distribution to a linear function. The fit has a slope of 0.244 ppm<sub>CH<sub>4</sub></sub> ppm<sub>C<sub>2</sub>H<sub>2</sub></sub><sup>-1</sup>, with an *R*<sup>2</sup> of 0.62. Given the release rate of 410 L h<sup>-1</sup> for C<sub>2</sub>H<sub>2</sub>, we find that the methane emissions from the degassing ponds are 1.13 kg d<sup>-1</sup>. We estimate the uncertainty of the emissions estimate to be about ±0.240 kg d<sup>-1</sup>. Given the wind direction, this emission number could include emissions from one or more of the clarification tanks, but since the clarification ponds were measured via floating chamber measurements to be just 0.26 kg d<sup>-1</sup> as a conservative upper limit, the emissions from the clarification tanks can be ignored.

For the tracer release with crossing of the plumes, which aimed to estimate the emissions for the whole plant, signals with a good correlation (> 0.6) between CH<sub>4</sub> and C<sub>2</sub>H<sub>2</sub> were integrated and the ratio of the areas calculated. As C<sub>2</sub>H<sub>2</sub> background is zero, there was no need to subtract it. However, for CH<sub>4</sub>, the lowest values between two crossings of the plumes could change a lot, depending on the wind direction. The results are summed up in Table 3. During the two days, two different C<sub>2</sub>H<sub>2</sub> emission rates were used, 10.320 and 27.840 kg d<sup>-1</sup> respectively. We observe a large variability (approximately 40 %) between the plumes and between the two days. The average value over the two days is 42 ± 12 kg d<sup>-1</sup> or 102 ± 29 g yr<sup>-1</sup> per inhabitant. The error here represent the standard deviation of the measurements and include therefore also the emission variability. Part of this variability is probably due to the background definition of the signals as well as the difficulty of sampling the plumes. It can also correspond to real variations in emissions with for example different emitting processes being switched on and off. We can then assume that the emissions from the plant, if these measurements are representative, are ranging from 30 to 54 kg d<sup>-1</sup> with a 40 % uncertainty at most.







## References

- Biraud, S., Ciais, P., Ramonet, M., Simmonds, P., Kazan, V., Monfray, P., O'Doherty, S., Spain, T. G., and Jennings, S. G.: European greenhouse gas emissions estimated from continuous atmospheric measurements and radon 222 at Mace Head, Ireland, *J. Geophys. Res.-Atmos.*, 105, 1351–1366, 2000. 9192
- 5 Cakir, F. and Stenstrom, M.: Greenhouse gas production: a comparison between aerobic and anaerobic wastewater treatment technology, *Water Res.*, 39, 4197–4203, doi:10.1016/j.watres.2005.07.042, 2005. 9184
- Chen, H., Winderlich, J., Gerbig, C., Hoefler, A., Rella, C. W., Crosson, E. R., Van Pelt, A. D.,  
10 Steinbach, J., Kolle, O., Beck, V., Daube, B. C., Gottlieb, E. W., Chow, V. Y., Santoni, G. W., and Wofsy, S. C.: High-accuracy continuous airborne measurements of greenhouse gases (CO<sub>2</sub> and CH<sub>4</sub>) using the cavity ring-down spectroscopy (CRDS) technique, *Atmos. Meas. Tech.*, 3, 375–386, doi:10.5194/amt-3-375-2010, 2010. 9189
- CITEPA: Rapport national pour la France au titre de la convention cadre des Nations  
15 Unis sur le changement climatique et du protocole de Kyoto, Source CITEPA/rapport CCNUCC édition de mars 2013, 66191 pp., available at: <http://www.citepa.org/fr/inventaires-etudes-et-formations/inventaires-des-emissions/ccnucc> (last access: 24 October 2013), 2013. 9184
- Crosson, E. R.: A cavity ring-down analyzer for measuring atmospheric levels of methane,  
20 carbon dioxide, and water vapor, *Appl. Phys. B*, 92, 403–408, doi:10.1007/s00340-008-3135-y, 2008. 9189
- Czepiel, P. M., Crill, P. M., and Harriss, R. C.: Methane emissions from municipal wastewater treatment processes, *Environ. Sci. Technol.*, 27, 2472–2477, doi:10.1021/es00048a025, 1993. 9184
- 25 Czepiel, P. M., Mosher, B., Harriss, R. C., Shorter, J. H., McManus, J. B., Kolb, C. E., Allwine, E., and Lamb, B. K.: Landfill methane emissions measured by enclosure and atmospheric tracer methods, *J. Geophys. Res.-Atmos.*, 101, 16711–16719, doi:10.1029/96JD00864, 1996. 9194
- Daelman, M. R. J., van Voorthuizen, E. M., van Dongen, U. G. J. M., Volcke, E. I. P., and van  
30 Loosdrecht, M. C. M.: Methane emission during municipal wastewater treatment, *Water Res.*, 46, 3657–3670, doi:10.1016/j.watres.2012.04.024, 2012. 9184, 9204

## AMTD

6, 9181–9224, 2013

### CH<sub>4</sub> local emissions measurements

C. E. Yver-Kwok et al.

Title Page

Abstract

Introduction

Conclusions

References

Tables

Figures

◀

▶

◀

▶

Back

Close

Full Screen / Esc

Printer-friendly Version

Interactive Discussion



**CH<sub>4</sub> local emissions measurements**

C. E. Yver-Kwok et al.

Title Page

Abstract

Introduction

Conclusions

References

Tables

Figures

◀

▶

◀

▶

Back

Close

Full Screen / Esc

Printer-friendly Version

Interactive Discussion



- El-Fadel, M. and Massoud, M.: Methane emissions from wastewater management, *Environ. Pollut.*, 114, 177–185, doi:10.1016/S0269-7491(00)00222-0, 2001. 9184
- Fang, S.-X., Zhou, L.-X., Masarie, K. A., Xu, L., and Rella, C. W.: Study of atmospheric CH<sub>4</sub> mole fractions at three WMO/GAW stations in China, *J. Geophys. Res.-Atmos.*, 118, 4874–4886, doi:10.1002/jgrd.50284, 2013. 9189
- Frankignoulle, M.: Field measurements of air-sea CO<sub>2</sub> exchange, *Limnol. Oceanogr.*, 33, 313–322, 1988. 9191
- Fredenslund, A. M., Scheutz, C., and Kjeldsen, P.: Tracer method to measure landfill gas emissions from leachate collection systems, *Waste Manage.* 30, 2146–2152, doi:10.1016/j.wasman.2010.03.013, 2010. 9194
- Galle, B., Samuelsson, J., Svensson, B. H., and Börjesson, G.: Measurements of methane emissions from landfills using a time correlation tracer method based on FTIR absorption spectroscopy, *Environ. Sci. Technol.*, 35, 21–25, doi:10.1021/es0011008, 2001. 9194
- Griffith, D. W. T., Deutscher, N. M., Caldow, C., Kettlewell, G., Rigggenbach, M., and Hammer, S.: A Fourier transform infrared trace gas and isotope analyser for atmospheric applications, *Atmos. Meas. Tech.*, 5, 2481–2498, doi:10.5194/amt-5-2481-2012, 2012. 9187
- Hammer, S. and Levin, I.: Seasonal variation of the molecular hydrogen uptake by soils inferred from continuous atmospheric observations in Heidelberg, southwest Germany, *Tellus B*, 61, 556–565, 2009. 9192
- Hammer, S., Griffith, D. W. T., Konrad, G., Vardag, S., Caldow, C., and Levin, I.: Assessment of a multi-species in situ FTIR for precise atmospheric greenhouse gas observations, *Atmos. Meas. Tech.*, 6, 1153–1170, doi:10.5194/amt-6-1153-2013, 2013. 9187
- Levin, I., Glatzel-Mattheier, H., Marik, T., Cuntz, M., Schmidt, M., and Worthy, D. E.: Verification of German methane emission inventories and their recent changes based on atmospheric observations, *J. Geophys. Res.*, 104, 3447–3456, 1999. 9192
- Levin, I., Born, M., Cuntz, M., Langendörfer, U., Mantsch, S., Naegler, T., Schmidt, M., Varlagin, A., Verclas, S., and Wagenbach, D.: Observations of atmospheric variability and soil exhalation rate of radon-222 at a Russian forest site. Technical approach and deployment for boundary layer studies, *Tellus B*, 54, 462–475, doi:10.1034/j.1600-0889.2002.01346.x, 2002. 9190
- Messenger, C., Schmidt, M., Ramonet, M., Bousquet, P., Simmonds, P., Manning, A., Kazan, V., Spain, G., Jennings, S. G., and Ciais, P.: Ten years of CO<sub>2</sub>, CH<sub>4</sub>, CO and N<sub>2</sub>O fluxes over

**CH<sub>4</sub> local emissions measurements**

C. E. Yver-Kwok et al.

Title Page

Abstract

Introduction

Conclusions

References

Tables

Figures

◀

▶

◀

▶

Back

Close

Full Screen / Esc

Printer-friendly Version

Interactive Discussion



Western Europe inferred from atmospheric measurements at Mace Head, Ireland, *Atmos. Chem. Phys. Discuss.*, 8, 1191–1237, doi:10.5194/acpd-8-1191-2008, 2008. 9192

Olivier, J. G. J., Bouwman, A. F., van der Maas, C. W. M., Berdowski, J. J. M., Veldt, C., Bloos, J. P. J., Visschedijk, A. J. H., Zandveld, P. Y. J., and Haverlag, J. L.: Description of EDGAR Version 2.0: A set of global emission inventories of greenhouse gases and ozone-depleting substances for all anthropogenic and most natural sources on a per country basis and on 1 degree × 1 degree grid, Rijksinstituut voor Volksgezondheid en Milieu RIVM, the Netherlands, 1996. 9203

Rella, C. W., Chen, H., Andrews, A. E., Filges, A., Gerbig, C., Hatakka, J., Karion, A., Miles, N. L., Richardson, S. J., Steinbacher, M., Sweeney, C., Wastine, B., and Zellweger, C.: High accuracy measurements of dry mole fractions of carbon dioxide and methane in humid air, *Atmos. Meas. Tech.*, 6, 837–860, doi:10.5194/amt-6-837-2013, 2013. 9189

Schery, S. D., Gaedert, D. H., and Wilkening, M. H.: Factors affecting exhalation of radon from a gravelly sandy loam, *J. Geophys. Res.-Atmos.*, 89, 7299–7309, 1984. 9190

Schmidt, M., Glatzel-Mattheier, H., Sartorius, H., Worthy, D. E., and Levin, I.: Western European N<sub>2</sub>O emissions – a top-down approach based on atmospheric observations, *J. Geophys. Res.*, 106, 5507–5516, 2001. 9192, 9193, 9194

Spokas, K., Bogner, J., Chanton, J., Morcet, M., Aran, C., Graff, C., Golvan, Y. M.-L., and Hebe, I.: Methane mass balance at three landfill sites: what is the efficiency of capture by gas collection systems?, *Waste Manage.*, 26, 516–525, doi:10.1016/j.wasman.2005.07.021, 2006. 9194

Szegvary, T., Conen, F., and Ciais, P.: European <sup>222</sup>Rn inventory for applied atmospheric studies, *Atmos. Environ.*, 43, 1536–1539, doi:10.1016/j.atmosenv.2008.11.025, 2009. 9193

Wang, J., Zhang, J., Xie, H., Qi, P., Ren, Y., and Hu, Z.: Methane emissions from a full-scale A/A/O wastewater treatment plant, *Bioresource Technol.*, 102, 5479–5485, doi:10.1016/j.biortech.2010.10.090, 2011. 9184

Winderlich, J., Chen, H., Gerbig, C., Seifert, T., Kolle, O., Lavrič, J. V., Kaiser, C., Höfer, A., and Heimann, M.: Continuous low-maintenance CO<sub>2</sub>/CH<sub>4</sub>/H<sub>2</sub>O measurements at the Zotino Tall Tower Observatory (ZOTTO) in Central Siberia, *Atmos. Meas. Tech.*, 3, 1113–1128, doi:10.5194/amt-3-1113-2010, 2010. 9189

WMO: 16th WMO/IAEA Meeting on Carbon Dioxide, Other Greenhouse Gases, and Related Measurement Techniques (GGMT-2011), available at: [http://www.wmo.int/pages/prog/arep/gaw/documents/Final\\_GAW\\_206\\_web.pdf](http://www.wmo.int/pages/prog/arep/gaw/documents/Final_GAW_206_web.pdf) (last access: 24 October 2013), 2011. 9196

Yver, C., Schmidt, M., Bousquet, P., Zahorowski, W., and Ramonet, M.: Estimation of the molecular hydrogen soil uptake and traffic emissions at a suburban site near Paris through hydrogen, carbon monoxide, and radon-222 semicontinuous measurements, *J. Geophys. Res.*, 114, D18304, doi:10.1029/2009JD012122, 2009. 9192, 9193

**AMTD**

6, 9181–9224, 2013

---

## **CH<sub>4</sub> local emissions measurements**

C. E. Yver-Kwok et al.

---

Title Page

Abstract

Introduction

Conclusions

References

Tables

Figures

◀

▶

◀

▶

Back

Close

Full Screen / Esc

Printer-friendly Version

Interactive Discussion



## CH<sub>4</sub> local emissions measurements

C. E. Yver-Kwok et al.

Title Page

Abstract

Introduction

Conclusions

References

Tables

Figures

◀

▶

◀

▶

Back

Close

Full Screen / Esc

Printer-friendly Version

Interactive Discussion



**Table 1.** Instruments used during the campaign and their specifications.

Instrument	Integration time used in the study	Species	Uncertainty for species of interest
FTIR LSCE	1 min/30 min	CO <sub>2</sub> , CH <sub>4</sub> , N <sub>2</sub> O, CO and δ <sup>13</sup> C	<0.1 % (CH <sub>4</sub> )
FTIR Bremen	5 min	CO <sub>2</sub> , CH <sub>4</sub> , N <sub>2</sub> O, CO and δ <sup>13</sup> C	<0.1 % (CH <sub>4</sub> )
CRDS	10 s/1 min	CH <sub>4</sub> , CO <sub>2</sub> , C <sub>2</sub> H <sub>2</sub> , H <sub>2</sub> O	<2 % (CH <sub>4</sub> ), <10 % (C <sub>2</sub> H <sub>2</sub> )
Radon analyzer	30 min	<sup>222</sup> Rn	less than 20 %
Weather station	1 min	Wind speed, wind direction, temperature, relative humidity and atmospheric pressure	3 %, 3°, 0.3 °C, 3 %, 0.05 %

**CH<sub>4</sub> local emissions measurements**

C. E. Yver-Kwok et al.

Title Page

Abstract

Introduction

Conclusions

References

Tables

Figures

◀

▶

◀

▶

Back

Close

Full Screen / Esc

Printer-friendly Version

Interactive Discussion

**Table 2.** Fluxes measured during chamber measurements on the clarification pond.

	Chamber Run No.	Mixer	CH <sub>4</sub> Flux (kg <sub>CH<sub>4</sub></sub> d <sup>-1</sup> )
Diffusive emissions <sup>a</sup>	2	Off	0.003 ± 0.0002
	3	Off	0.003 ± 0.0002
	4	Off	0.005 ± 0.0003
	7	On	0.012 ± 0.0007
Erratic emissions <sup>b</sup>	1	Off	0.165 ± 0.011
	5	On	0.257 ± 0.016
	8	On	0.111 ± 0.007
	9	On	0.028 ± 0.002

<sup>a</sup> The fluxes were calculated by a linear fit, because diffusive flux could be assumed.

<sup>b</sup> The observed concentration increase was not linear. The numbers are based on a linear fit of the steepest increase over a 10 min period. The fluxes calculated then represent an upper limit.



CH<sub>4</sub> local emissions measurements

C. E. Yver-Kwok et al.

**Table 4.** Summary of the results from the process to the regional scale. The given uncertainties were determined in different ways. Refer to the main text for details.

	Clarification Ponds (3)	Aeration Ponds (2) non-aeration area	Aeration Ponds (2) aeration area	Degassing Pond (1)	Station	Surrounding – City of Valence
CH <sub>4</sub> emissions (kg <sub>CH<sub>4</sub></sub> d <sup>-1</sup> )	0.02 ± 0.01  + emissions by erratic events (at most 0.771 ± 0.05)	0.08 ± 0.004  + emissions by erratic events (not determined)	1.32 ± 0.01	1.13 ± 0.24	41.97 ± 11.47	1500.00 (uncertainty not determined)

Title Page

Abstract

Introduction

Conclusions

References

Tables

Figures

I◀

▶I

◀

▶

Back

Close

Full Screen / Esc

Printer-friendly Version

Interactive Discussion



## CH<sub>4</sub> local emissions measurements

C. E. Yver-Kwok et al.

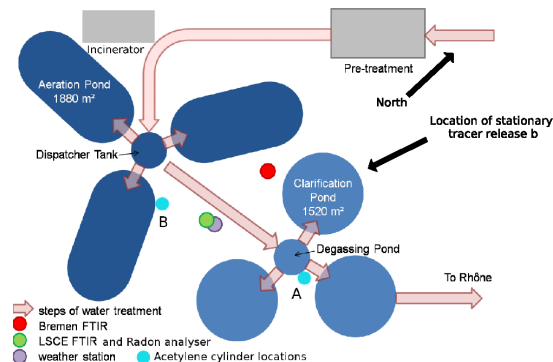


**Fig. 1.** First panel: Aerial view (Google map) of the waste water treatment plant. Second panel: Schematic view of the waste water treatment plant.

Title Page	
Abstract	Introduction
Conclusions	References
Tables	Figures
◀	▶
◀	▶
Back	Close
Full Screen / Esc	
Printer-friendly Version	
Interactive Discussion	



**CH<sub>4</sub> local emissions measurements**

C. E. Yver-Kwok et al.

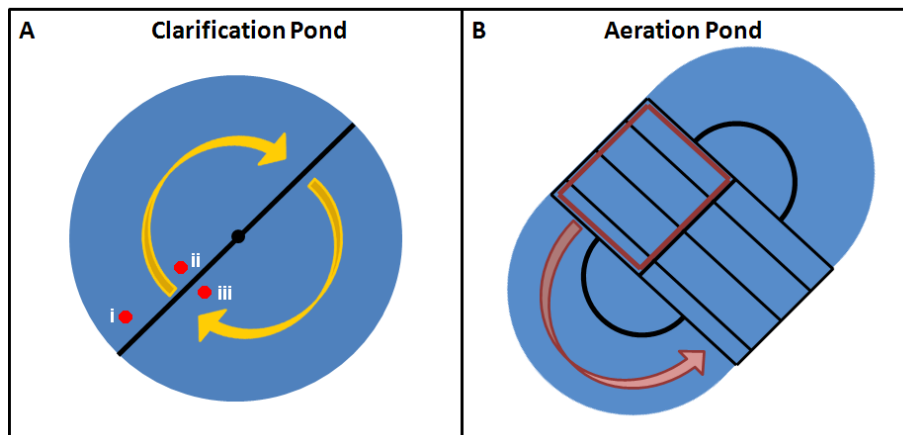


**Fig. 2.** Schematic of the two basins that were measured with the floating chamber. **(A)** clarification pond, the yellow arrow shows the direction in which the arm rotates. The red dots and symbols refer to the location of the chamber during runs 1, 2, 3 (symbol i), 4, 5, 7 (symbol ii) and 6, 8, 9 (symbol iii). **(B)** aeration pond, the red rectangle denotes the aeration area, the arrow the water flow.

[Title Page](#)[Abstract](#)[Introduction](#)[Conclusions](#)[References](#)[Tables](#)[Figures](#)[◀](#)[▶](#)[◀](#)[▶](#)[Back](#)[Close](#)[Full Screen / Esc](#)[Printer-friendly Version](#)[Interactive Discussion](#)

CH<sub>4</sub> local emissions measurements

C. E. Yver-Kwok et al.

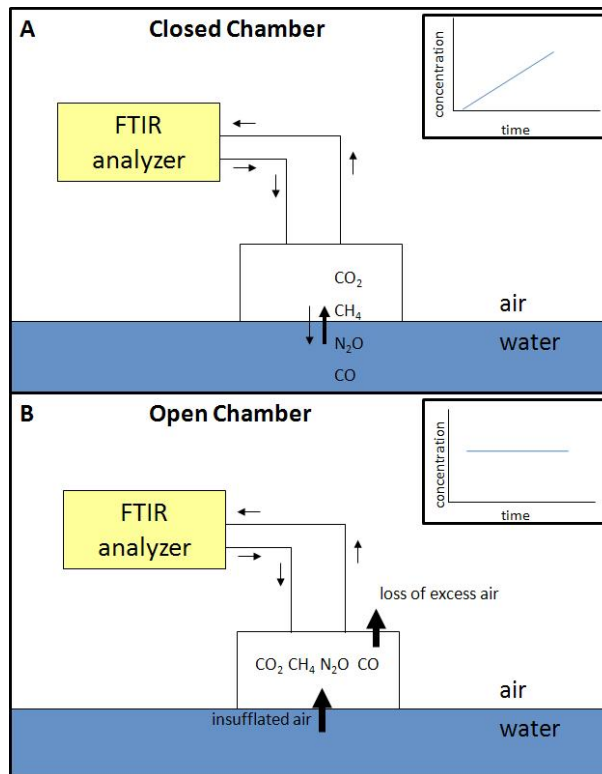


**Fig. 3.** Schematic showing different modes of chamber employment. **(A)** Conventional floating chamber used on a calm surface (accumulation closed-chamber measurements). The schematic concentration vs. time points out how the gas accumulates in the chamber over time (in case of a positive net flux from water to air). This increase is linearly approximated and from the slope, the flux is calculated. **(B)** Flow-through open chamber, the excess air escapes and the concentration measured in the chamber relates directly to the concentration in the emitted air. Thus, here, we refer to the concentration reached in one time interval.

**CH<sub>4</sub> local emissions measurements**

C. E. Yver-Kwok et al.

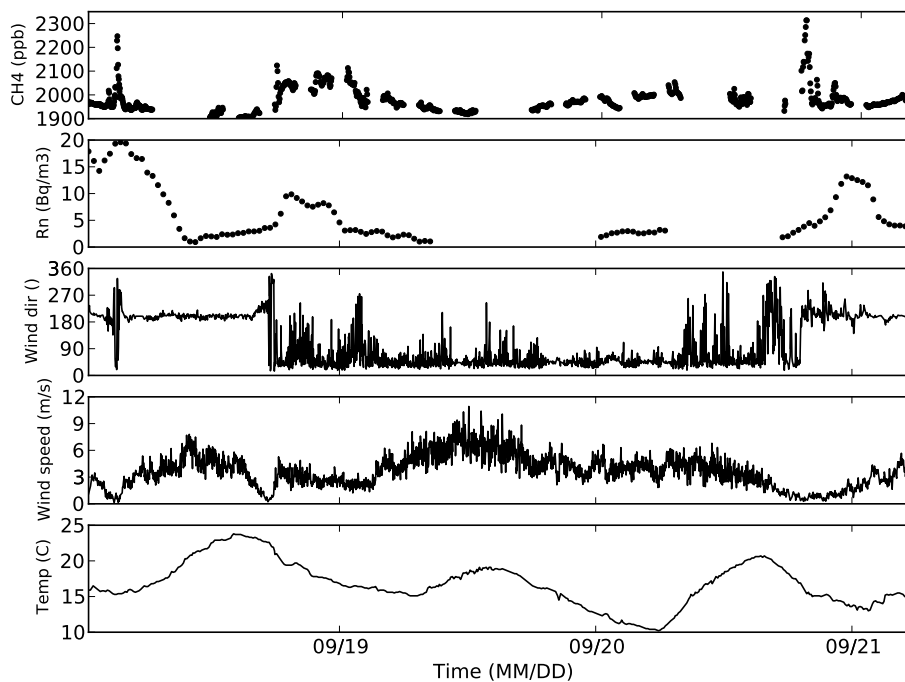
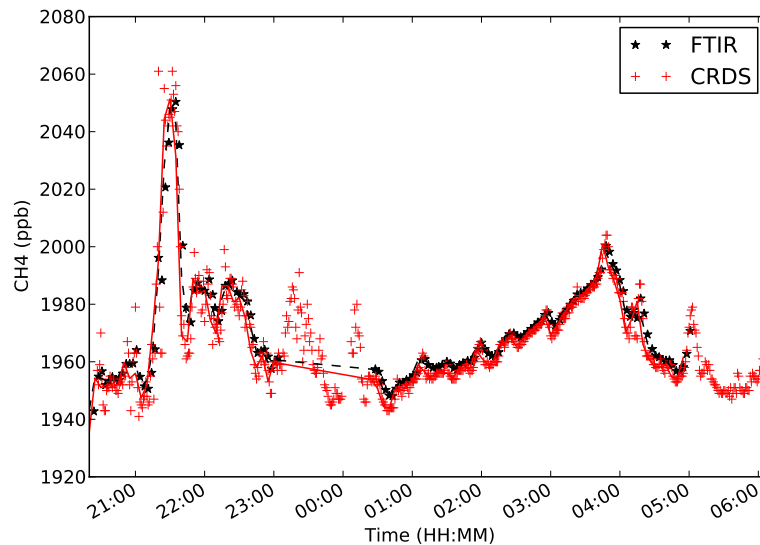


**Fig. 4.** CH<sub>4</sub> concentrations from the LSCE FTIR analyzer, <sup>222</sup>Rn activity, wind speed, wind direction and temperature during the campaign.

[Title Page](#)[Abstract](#)[Introduction](#)[Conclusions](#)[References](#)[Tables](#)[Figures](#)[◀](#)[▶](#)[◀](#)[▶](#)[Back](#)[Close](#)[Full Screen / Esc](#)[Printer-friendly Version](#)[Interactive Discussion](#)

**CH<sub>4</sub> local emissions measurements**

C. E. Yver-Kwok et al.

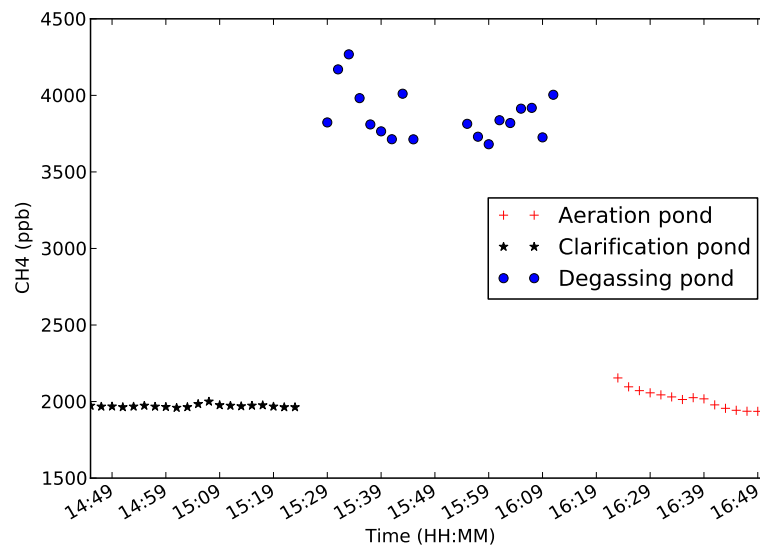


**Fig. 5.** Comparison of CH<sub>4</sub> concentrations from the LSCE FTIR and CRDS analyzers over the night of 20 September.

[Title Page](#)[Abstract](#)[Introduction](#)[Conclusions](#)[References](#)[Tables](#)[Figures](#)[◀](#)[▶](#)[◀](#)[▶](#)[Back](#)[Close](#)[Full Screen / Esc](#)[Printer-friendly Version](#)[Interactive Discussion](#)

**CH<sub>4</sub> local emissions measurements**

C. E. Yver-Kwok et al.

**Fig. 6.** CH<sub>4</sub> concentrations measured by the LSCE FTIR analyzer over the different ponds.[Title Page](#)[Abstract](#)[Introduction](#)[Conclusions](#)[References](#)[Tables](#)[Figures](#)[◀](#)[▶](#)[◀](#)[▶](#)[Back](#)[Close](#)[Full Screen / Esc](#)[Printer-friendly Version](#)[Interactive Discussion](#)

CH<sub>4</sub> local emissions measurements

C. E. Yver-Kwok et al.

Title Page

Abstract

Introduction

Conclusions

References

Tables

Figures

◀

▶

◀

▶

Back

Close

Full Screen / Esc

Printer-friendly Version

Interactive Discussion

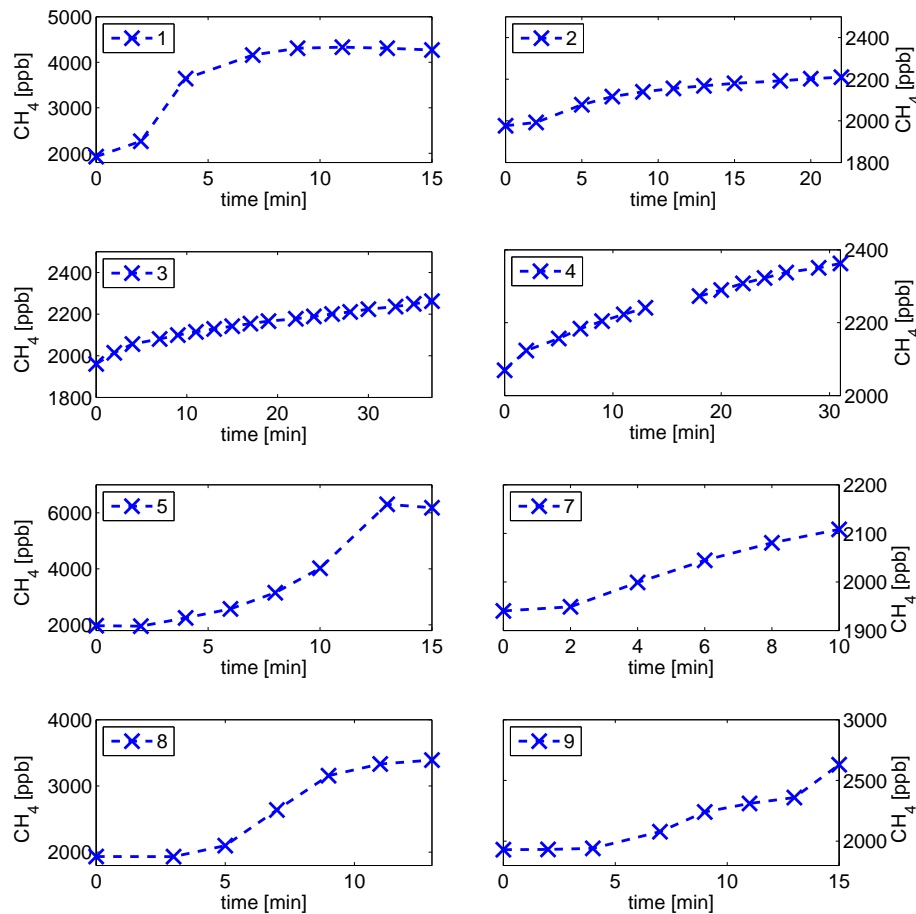


**Fig. 7.** Floating chamber experiments conducted on the clarification pond when the mixer was off (1–4) and on (5–9), respectively.

**CH<sub>4</sub> local emissions measurements**

C. E. Yver-Kwok et al.

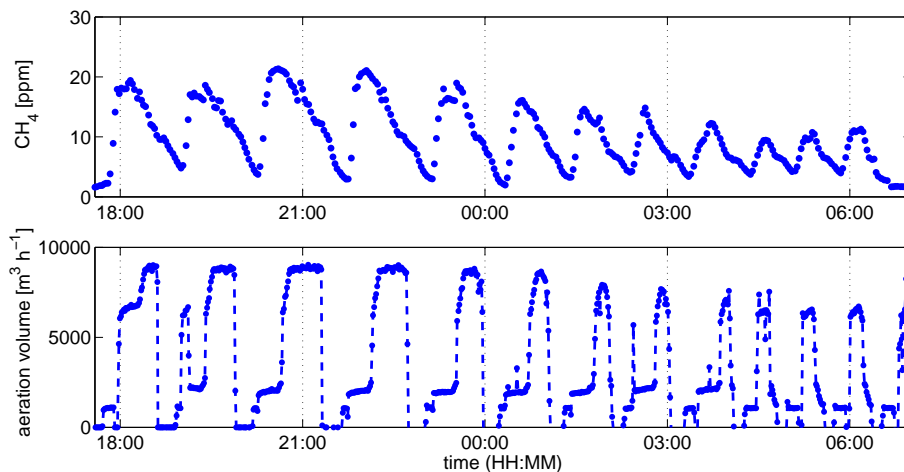


**Fig. 8.** Measurements in the aeration area of the pond. Upper panel: methane concentration vs. time. Lower panel: respective volume of injected air during the same time period.

[Title Page](#)[Abstract](#)[Introduction](#)[Conclusions](#)[References](#)[Tables](#)[Figures](#)[◀](#)[▶](#)[◀](#)[▶](#)[Back](#)[Close](#)[Full Screen / Esc](#)[Printer-friendly Version](#)[Interactive Discussion](#)

**CH<sub>4</sub> local emissions measurements**

C. E. Yver-Kwok et al.

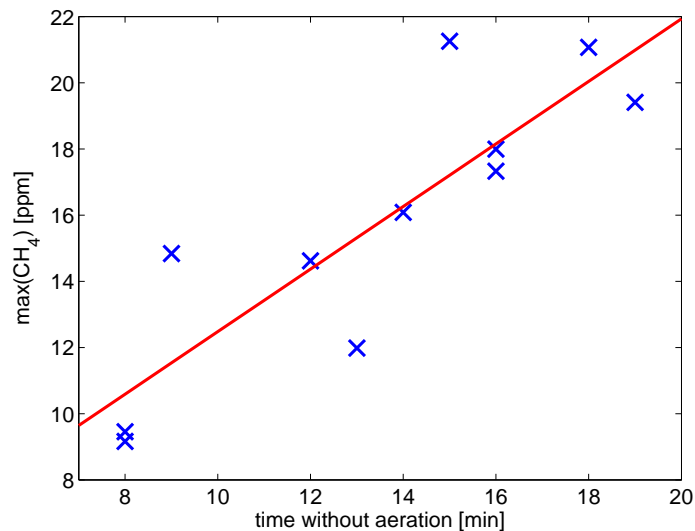


**Fig. 9.** Methane maxima reached during the night chamber measurement vs. time without aeration. Blue: measurements, red: linear fit.

[Title Page](#)[Abstract](#)[Introduction](#)[Conclusions](#)[References](#)[Tables](#)[Figures](#)[◀](#)[▶](#)[◀](#)[▶](#)[Back](#)[Close](#)[Full Screen / Esc](#)[Printer-friendly Version](#)[Interactive Discussion](#)

CH<sub>4</sub> local emissions measurements

C. E. Yver-Kwok et al.

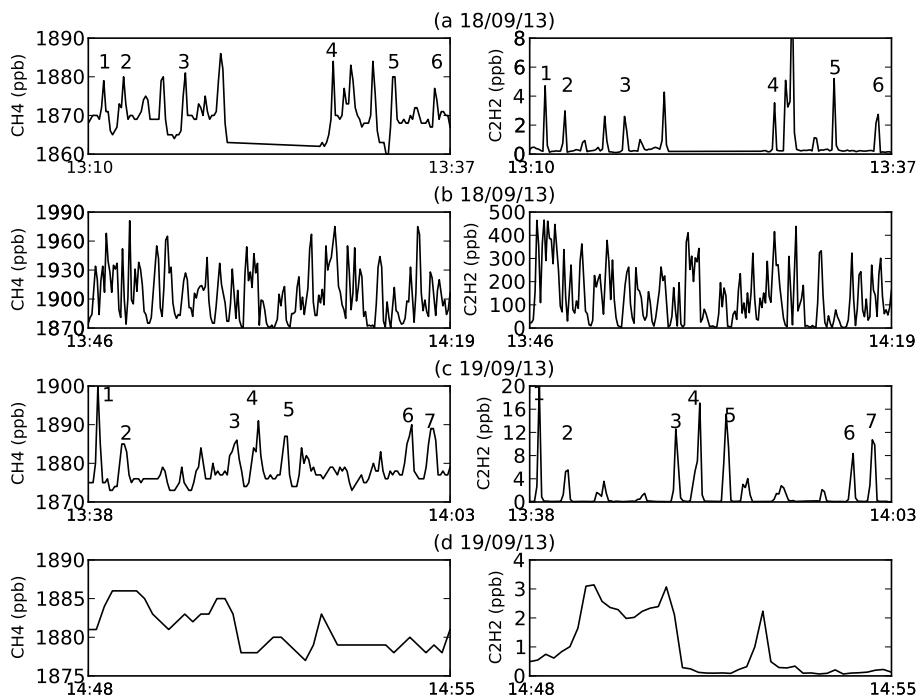


**Fig. 10.** Concentrations of CH<sub>4</sub> and C<sub>2</sub>H<sub>2</sub> during the four tracer release episodes. Episode **(a)**, estimation of the whole plant emission on 18 September with a south wind, C<sub>2</sub>H<sub>2</sub> cylinder located in A; Episode **(b)**, estimation of the degassing pond emissions on 18 September with a south wind, C<sub>2</sub>H<sub>2</sub> cylinder located in A; Episode **(c)**, estimation of the whole plant emissions on 19 September with a north wind, C<sub>2</sub>H<sub>2</sub> cylinder located in A; Episode **(d)**, estimation of the whole plant emissions on 19 September with a north wind, C<sub>2</sub>H<sub>2</sub> cylinder located in B. The numbers indicate the signals (peaks) that are correlated with each other with a correlation coefficient higher than 0.6, used to calculate the CH<sub>4</sub> emissions.

Title Page

Abstract

Introduction

Conclusions

References

Tables

Figures

◀

▶

◀

▶

Back

Close

Full Screen / Esc

Printer-friendly Version

Interactive Discussion



CH<sub>4</sub> local emissions measurements

C. E. Yver-Kwok et al.

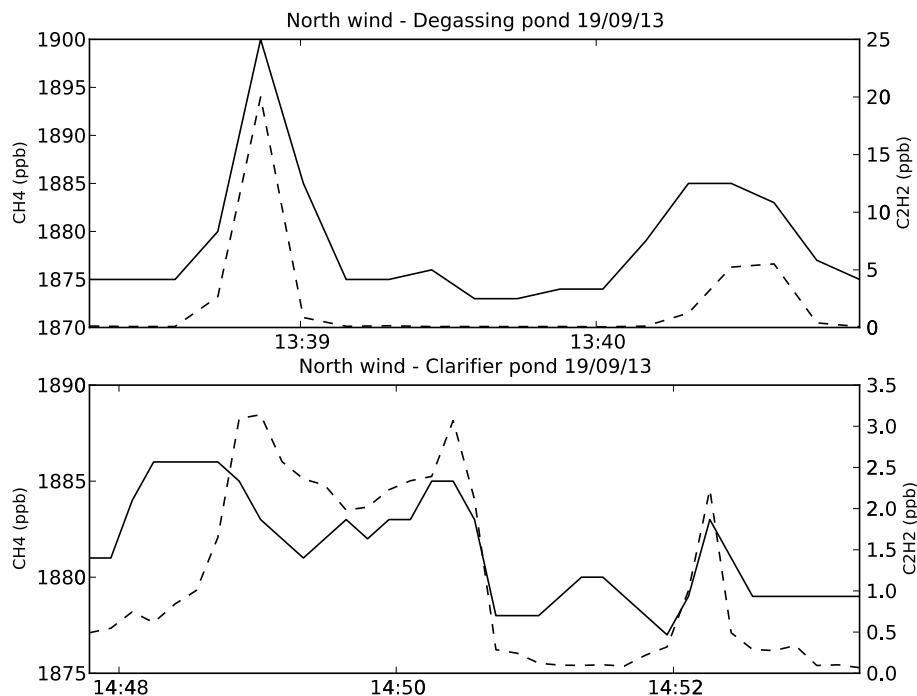


**Fig. 11.** Difference of correlation between CH<sub>4</sub> and C<sub>2</sub>H<sub>2</sub> depending on the location of the C<sub>2</sub>H<sub>2</sub> cylinder. Top, the cylinder was located near the degassing pond ((A) in Fig. 1) and the shifting in the signals indicates that the main emission source is west of the pond. Bottom, the cylinder is located near one of the clarification pond ((B) in Fig. 1), west of the previous location and there is no significant shifting anymore between the peaks.

Title Page

Abstract

Introduction

Conclusions

References

Tables

Figures

◀

▶

◀

▶

Back

Close

Full Screen / Esc

Printer-friendly Version

Interactive Discussion

